A Microvalve With Integrated Sensors and Customizable Normal State for Low-Temperature Operation

Jong M. Park, Allan T. Evans, Kristian Rasmussen, Tyler R. Brosten, Gregory F. Nellis, Sanford A. Klein, and Yogesh B. Gianchandani

***Abstract*—This paper reports on design, fabrication, and testing of a piezoelectrically actuated microvalve with integrated sensors for flow modulation at low temperatures. One envisioned application is to control the flow of a cryogen for distributed cooling with a high degree of temperature stability and a small thermal gradient. The valve consists of a micromachined die fabricated from a silicon-on-insulator wafer, a glass wafer, a commercially available piezoelectric stack actuator, and Macor ceramic encapsulation that has overall dimensions of $1.5 \times 1.5 \times 1.1$ cm^3. A piezoresistive pressure sensor and a thin-film Pt resistance temperature detector are integrated on the silicon die. The assembly process allows the implementation of normally open, partially open, and normally closed valves. At room temperature, gas flow modulation from 200 to 0 mL/min is achieved from 0- to 40-V actuation. Flow modulation at various temperatures from room temperature to 205 K is also reported. The pressure sensor has sensitivity of 356 ppm/kPa at room temperature, with temperature coefficient of sensitivity of −6507 ppm/K. The temperature sensor has sensitivity of 0.29%/K. The valve and the sensors are tested across a wide range of temperatures, and the effect of temperature on performance is discussed. [2008-0253]**

***Index Terms*—Cooling systems, cryogenic, microelectromechanical systems (MEMS), piezoelectric, piezoresistive pressure sensor, resistance temperature detector (RTD).**

I. Introduction

FUTURE SPACE missions will require cooling of large optical structures and cryogenic storage systems with a high degree of temperature stability and a small temperature gradient [1], [2]. One approach that is envisioned is a distributed network that can provide localized control over cooling elements throughout the system. These distributed cooling elements may each consist of actively controlled valves, integrated heat exchangers, and temperature sensors [Fig. 1(a)], and be positioned across the structure to efficiently achieve uniform cooling [Fig. 1(b)]. In order to realize such a distributed cooling system, it is essential to have actively controlled valves that work with liquids or gases across large temperature variations. The valves must provide a high degree of flow modulation for adequate cooling and should have a set initial opening that configures a default cooling architecture in case of power failure. The valves should also be able to withstand a large pressure difference, in order to accommodate the free expansion required in a Joule–Thompson cooling cycle.

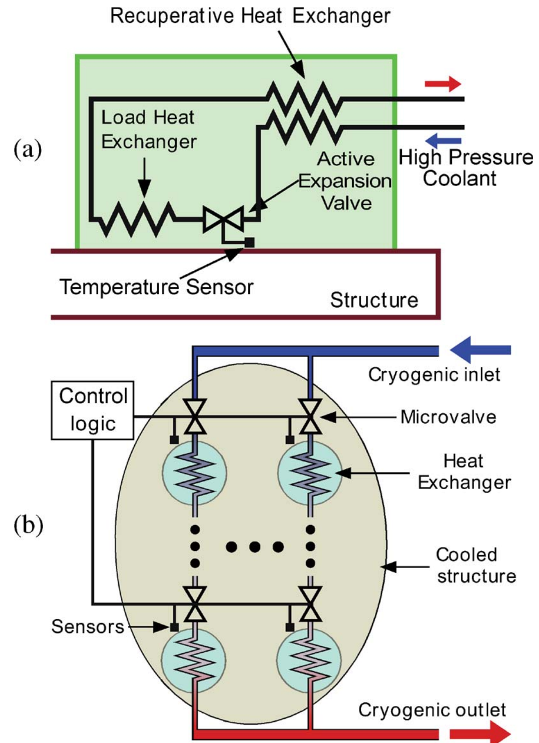

Fig. 1. Proposed application of actively controlled valve. (a) Microvalves can be used to modulate flow of coolant and used as expansion valves in Joule–Thompson cryocoolers. (b) Distributed cooling network: arrays of cooling elements are placed around a structure to be cooled.

Several valve actuation schemes can be considered. Electromagnetic actuation can create relatively large force and displacement, but at the expense of high power consumption [3]–[6]. Electrostatic actuation is characterized by a fast

Manuscript received October 6, 2008; revised February 12, 2009. First published June 5, 2009; current version published July 31, 2009. This work was supported by NASA under Award NNA05CP85G. Subject Editor F. Ayazi.

J. M. Park is with the Department of Electrical Engineering and Computer Science, University of Michigan, Ann Arbor, MI 48109 USA, and also with the Honeywell ACS Sensors and Wireless Laboratory, Plymouth, MN 55416 USA (e-mail: parkjong@umich.edu).

A. T. Evans and Y. B. Gianchandani are with the Department of Electrical Engineering and Computer Science, University of Michigan, Ann Arbor, MI 48109 USA (e-mail: evansall@umich.edu; yogesh@umich.edu).

K. Rasmussen, T. R. Brosten, G. F. Nellis, and S. A. Klein are with the Department of Mechanical Engineering, University of Wisconsin, Madison, WI 53706 USA (e-mail: tyler.brosten@coe.montana.edu; gfnellis@engr.wisc.edu; klein@engr.wisc.edu).

Color versions of one or more of the figures in this paper are available online at http://ieeexplore.ieee.org.

Digital Object Identifier 10.1109/JMEMS.2009.2021097

1057-7157/$26.00 © 2009 IEEE

Authorized licensed use limited to: University of Michigan Library. Downloaded on September 8, 2009 at 22:10 from IEEE Xplore. Restrictions apply.

response and low power consumption but typically does not provide adequate force against high inlet pressures. Furthermore, electrostatically driven valves are typically operated in binary mode rather than as proportional valves, and thus require for the use of an array to achieve graduated flow control [7]–[11]. Various forms of thermal actuation schemes, such as thermopneumatic [12], [13], bimetallic [14]–[16], and shape memory alloy [17], can produce considerable force and relatively large displacement. However, these have relatively high power consumption and slow response times, and their operation may generate parasitic heating in a cryogenic system. For this paper, piezoelectric actuation is used, to allow proportional flow control, to generate high force, and to minimize the power consumption. Piezoelectric microvalves without integrated sensors have been developed for space applications [18], [19] and in our previous work, they have been shown to work in a cryogenic environment [20].

In this paper, we describe a piezoelectrically actuated microvalve with integrated sensors that monitor inlet pressure and coolant temperature, and enable closed loop control of distributed cooling systems, in a compact form.[1] Both sensors must work with a mixed-phase heterogeneous coolant, maintaining accuracy across a wide temperature range. (In past efforts, microvalves were often integrated with flow sensors [22], [23]. For our application, measurement of the inlet pressure of the coolant provides adequate information.) The measured temperatures across the distributed network can be used by a controller to properly adjust cooling rates to various parts of the surface to provide a minimal thermal gradient. In addition, the results of the temperature sensor can be used to compensate for the temperature coefficients of the pressure sensor. This sensor integration is particularly significant in space missions, as the launch cost increases exponentially with mass.

The two main pressure sensing techniques that utilize membrane structures are piezoresistive sensing [24] and capacitive sensing [25]. The former, in a Wheatstone bridge configuration, was selected because it is more linear and has lower output impedance than capacitive readouts, allowing readout circuitry to be located remotely and sheltered from valve operating temperatures.

The most common tools for measuring cryogenic temperature are thermocouples, diodes, and resistance temperature detectors (RTDs) [26]. As the entire device is exposed to the operating temperature of the valve, the requirement of a temperature reference junction prevents the use of a thermocouple for the temperature sensor. Diode thermometry uses the temperature dependence of forward voltage drop in a p-n junction biased at constant current. However, this technique is very sensitive to the presence of radiation, due to charging of oxide layers, and electromagnetic interference that might be present in open space can create magnetic field-induced voltage across the junction [27]. An RTD temperature sensor works by sensing change in resistance with changing temperature. The platinum RTD is known to have excellent linearity down to 70 K, and measurement down to 14 K is routinely performed with appropriate calibration. A platinum RTD was selected as the temperature sensor for this work, because of its linear response in the range of our interest, industry-standard robustness, and ease of implementation.

[1] Portions of this paper were published in conference abstract form in [21].

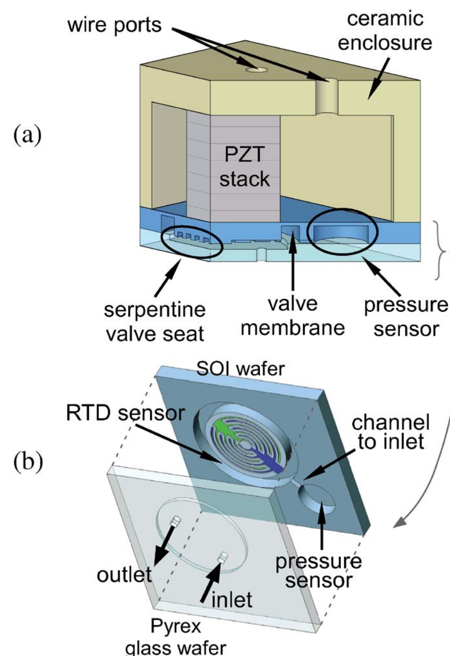

Fig. 2. Microvalve concept. (a) Cutaway view of assembled ceramic-PZT-Si-glass valve structure. (b) Valve plate suspended by Si membrane with integrated sensors viewed from the bottom. RTD sensor is located on the backside of the wafer and is not visible.

The valves described have a normal state that can be customized during assembly to provide the necessary default flow rate for every distributed element. A default network can be designed with valves that are normally open, normally closed, and partially open so that the coolant network still maintains some functionality in the case of complete power failure.

A general description of the device design and its operation is described in Section II. A numerical flow model specific to the valve and structural analysis are presented in Section III. The fabrication and assembly process is discussed in Section IV. Experimental results are reported in Section V, followed by discussion and conclusion in Sections VI and VII, respectively.

II. Device Structure and Operation

The device consists of three main components: a valve for flow modulation, a pressure sensor, and a temperature sensor for monitoring purposes. The valve operates by pressing a suspended silicon plate against a glass plate using out-of-plane piezoelectric actuation. Piezoelectric actuation provides enough force to displace the silicon plate against large inlet pressures (above 1 atm) with negligible dc power consumption and acceptable cryogenic performance. A multilayered lead zirconate titanate (PZT) stack (Physik Instrumente, Germany) with 5×5 mm^2 footprint and 6-mm height is used as an actuator. The valve die and the piezoelectric actuator are housed inside a Macor (machinable glass-mica ceramic) structure [Fig. 2(a)]. Macor is also used to create the fluidic header that is used

Authorized licensed use limited to: University of Michigan Library. Downloaded on September 8, 2009 at 22:10 from IEEE Xplore. Restrictions apply.

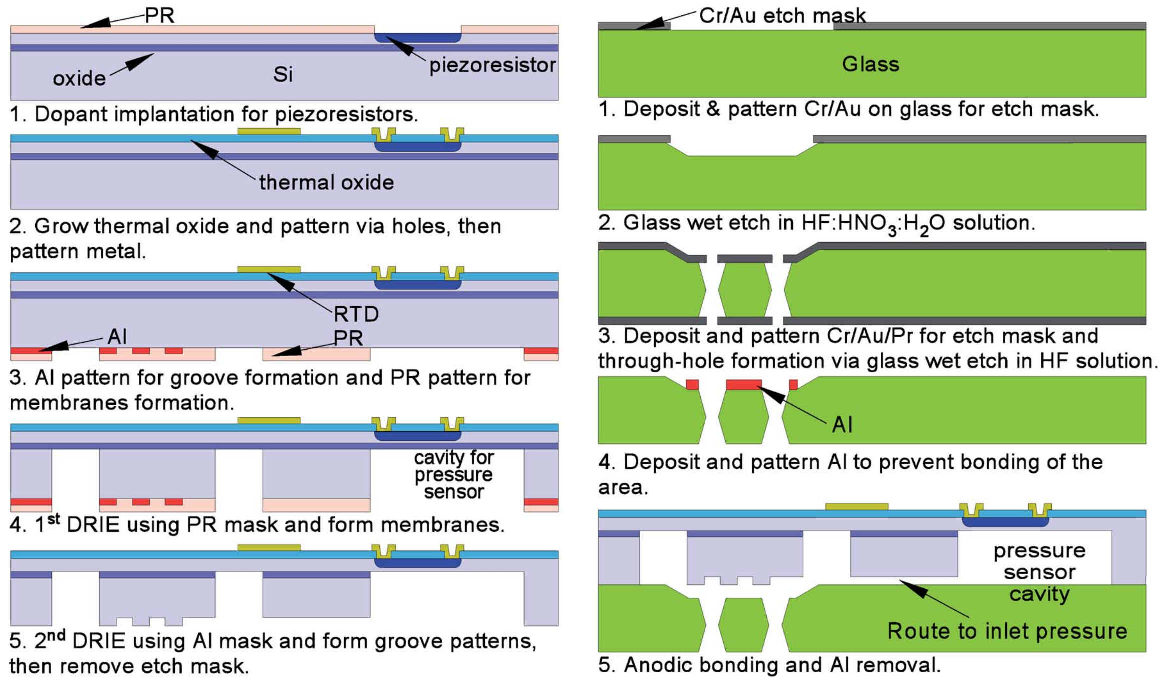

Fig. 3. Si-glass micromachining process. Sensors are formed on the device layer of the SOI wafer by various surface micromachining techniques. The buried oxide layer in SOI wafer acts as an etch stop for DRIE when forming membranes. A two-step DRIE process is illustrated for SOI wafer. A glass wafer undergoes two wet etch steps for a recess and through-hole formation. Next, the two wafers are anodically bonded and diced.

to connect the inlet and outlet of the valve to the rest of the flow path.

A small displacement provided by piezoelectric actuation is further reduced at cryogenic temperatures [28]. This limited displacement is compensated by perimeter augmentation of the valve flow passage. The flow area for an out-of-plane valve (A_{valve}) is given by the product of the valve stroke (δ) and the perimeter of the valve seat (p)

$$A_{\text{valve}} = \delta \cdot p. \tag{1}$$

A large p is used to compensate for a limited δ. Extended serpentine grooves ($>$ 30 cm in length) are fabricated on the valve plate as shown schematically in Fig. 2(b), to increase flow area. Each groove measures 50 μm wide and 120 μm deep.

The valve seat presented here has a membrane suspension. There are several advantages provided by this design compared to a valve with flexure-type suspension. The membrane suspension prevents the fluid from entering the package cavity, and thereby greatly reduces the dead volume of the valve. The dead volume in the device is only 0.021 cm^3, which is less than 1% of the total valve volume. The membrane suspension is fabricated using a process that is very easy to integrate with a diaphragm pressure sensor. A channel is constructed to route the inlet fluid pressure to the pressure-sensing element. The thin silicon membrane between the flow path and strategically placed temperature sensor provides a path with a relatively small thermal resistance to the fluid, while preventing direct contact with it (Figs. 2–4).

The membrane of the pressure sensor is designed to measure and withstand up to 3 atm of differential pressure. It has four boron-doped piezoresistors on a silicon diaphragm, which

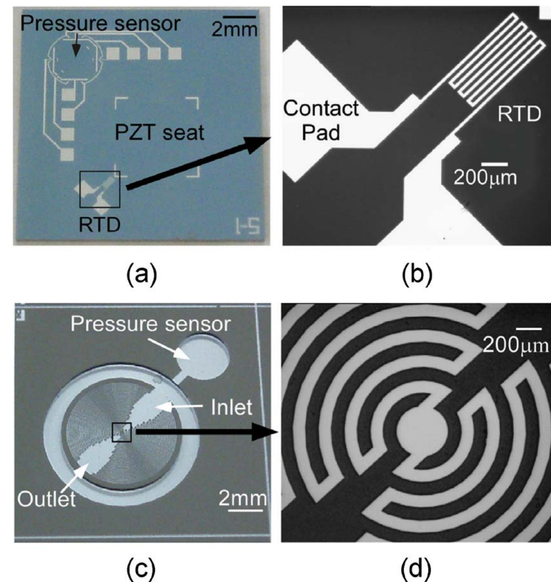

Fig. 4. (a) Photograph of the top of the SOI wafer showing metal contact layer with (b) an expanded view of the platinum RTD. (c) Wide and (d) expanded views of the circular serpentine groove patterns for perimeter augmentation from the bottom of the SOI wafer. This side bonds to the glass wafer.

occupy a surface area of 0.09 mm^2. The resistors have a target sheet resistance of about 2.97×10^3 $\Omega/\square$ and a resistance of 26.7 kΩ. As noted previously, the resistors are arranged in a Wheatstone bridge configuration.

A 100-nm-thick platinum film is used for the temperature sensor. To achieve approximately 400 Ω of resistance, 20-μm width, 7-mm-long thin-film platinum is patterned in serpentine shape on a valve membrane.

Authorized licensed use limited to: University of Michigan Library. Downloaded on September 8, 2009 at 22:10 from IEEE Xplore. Restrictions apply.

III. Modeling

A numerical flow model, specific to the perimeter-augmented microvalve, has been developed to examine the flow behavior of the valve. The flow through the valve is assumed to be isothermal, laminar, and steady flow. The governing flow equations are specific to each flow domain. The flow model predictions are compared to experimental measurements in Section V. A brief summary of the salient model aspect follows. More detail on the model development and verification can be found in [29].

Flow through the grooves (which are recessed regions) is governed by the phenomenological equation [30]

$$-\frac{dP_{\rm g}}{dx} = \frac{f}{D_{\rm h}}\frac{\rho}{2}V_{\rm g}^2 + \rho V_{\rm g}\frac{dV_{\rm g}}{dx} \quad (2)$$

where $P_{\rm g}$ and $V_{\rm g}$ are the pressure and velocity of the fluid or gas within a groove, f is an empirically determined friction factor, $D_{\rm h}$ is the groove hydraulic diameter, and ρ is the density. The empirical friction factor was determined by successive adjustment of the boundary conditions for an idealized 3-D groove modeled using FLUENT 6.2.

At small values of the valve seat displacement, values of the Knudsen number based on the valve seat clearance greater than 0.1 are expected. As a result, a departure from no slip conditions at the upper and lower walls of the land can occur. Furthermore, for gases at high flow rates across the land, compressibility effects can become significant. Therefore, a 1-D equation accounting for slip and compressibility effects was chosen to govern flow across the land [31]

$$\dot{m}' = \frac{\delta^3 P_{\rm o}^2}{24\mu LRT}\left[P_{\rm r}^2 - 1 + 12K_{\rm n}(P_{\rm r}-1)\right] \quad (3)$$

where $\dot{m}'$ is the mass flow rate per unit channel width, δ is the gap height, $P_{\rm o}$ is the outlet pressure, μ is viscosity of the fluid, L is the channel length, R is the ideal gas constant, T is the temperature, $K_{\rm n}$ is the Knudsen number evaluated at the land exit based on δ, and $P_{\rm r}$ is the ratio of inlet pressure to the outlet pressure. The nonlinear nature of (2) and (3) suggest that a linear scaling of the total valve flow rate with flow area and pressure difference across the valve inlet and outlet is limited to low flow speeds across the land and within the grooves. Continuity is applied to the component level models, and the resulting system of equations is solved using the Engineering Equation Solver [32].

The structural response of the valve diaphragms to internal pressurization and innate thermal stresses was studied using the finite element analysis tool, ANSYS. For the valve diaphragm that has outer radius of 4.7 mm and inner radius of 3.6 mm, the spring constant is approximately 3.8×10^6 N/m. In addition to internal pressurization loads, thermal stresses exist on the membrane in the working environment, because the silicon valve seat is bonded to the perforated glass substrate at 400 °C, while the valve is designed to operate primarily at cryogenic temperatures. Using the thermal expansion coefficients of silicon [33] and glass [34] at various temperatures, stress on the membrane was evaluated at -150 °C. In the worst case scenario of 6-μm maximum displacement and 10 atm of internal pressure, the maximum stress within the membrane was estimated to be 0.5 GPa, which is a fraction of the yield strength of silicon ($\approx$7 GPa). The structural study concluded the membrane design has suitable integrity to be used within the targeted design criteria.

IV. Device Fabrication

The fabrication process is a variant of the process previously used to create flexure suspended microvalves [20]. Steps have been added to the process to create the embedded sensors, and other steps have been altered to increase yield and decrease process complexity. The valve is fabricated from a silicon-on-insulator (SOI) wafer with layer thicknesses of 50-μm Si, 0.5-μm SiO_2, and 450-μm Si, and a 500-μm-thick Pyrex glass wafer. The SOI and glass wafers are independently processed, bonded, and then cut into individual die prior to assembly with the PZT stack, and packaging within the ceramic capsule. The fabrication processes for SOI and glass wafers are illustrated in Fig. 3.

First, boron implantation of 1×10^{14} cm^{-2} dose at 10 keV is performed to form piezoresistors (Innovion Corporation, Chandler, AZ). (The implantation dose and energy are selected to yield the correct carrier profile after implantation and annealing using the T-SUPREM 4 implantation simulator.) A thermal oxide is grown to both provide the necessary isolation and act as the high-temperature anneal needed to activate and diffuse the implanted boron. A 2000-Å oxide is grown at 1000 °C for 50 min, and the wafer is left at the temperature additional 20 min in nitrogen environment to allow for enough diffusion time for the implanted boron.

After the thermal oxidation and anneal, vias are etched in the oxide using buffered hydrofluoric acid (BHF) to create contacts to the piezoresistors, and Ti/Pt layer is deposited on the wafers to form the RTD. Lastly, gold is deposited on the contact pads for easier electrical contact with external wiring. Fig. 4 shows the fabricated die with pressure and temperature sensors.

After the device side is processed, the back side of the wafer undergoes a two-step deep reactive ion etch (DRIE) process to create the pressure sensor diaphragm, the membrane suspension, and the serpentine groves that increase the flow perimeter. An Al layer is patterned with liftoff process and photoresist (PR) is subsequently patterned on top of the Al pattern. The PR, which covers a region wider than the Al layer does, acts as an etch mask for the first DRIE step that is approximately 400 μm deep. This forms the valve membrane and pressure sensor cavity. Next, the PR is removed, and Al is used as an etch mask for the final DRIE step which engraves serpentine grooves for perimeter augmentation. Fig. 4(c) and (d) shows the bottom view of the silicon die after these processes. The resulting grooves are 120 μm in depth and provide seat perimeters that are longer than 30 cm in length to provide larger flow area when the valve opens.

A Pyrex glass wafer is first patterned with 2-μm-deep wet-etched recesses to accommodate the PZT displacement. This is done using a Cr/Au and PR mask in diluted HF (H_2O : HF : HNO_3 $= 10 : 7 : 3$). The HF attacks the Si–O bond and etches SiO_2, which is a major content in glass substrate. The rest of

Authorized licensed use limited to: University of Michigan Library. Downloaded on September 8, 2009 at 22:10 from IEEE Xplore. Restrictions apply.

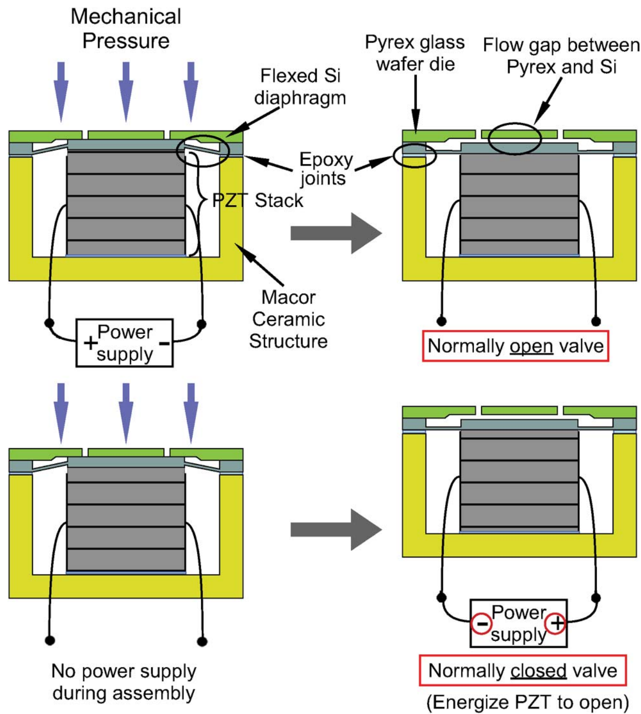

Fig. 5. Assembly process can be slightly modified to result in either normally closed or normally open valve. Energizing the PZT actuator during assembly results in (top) normally open configuration, while no PZT actuation during assembly yields (bottom) normally closed valve. For normally closed valve configuration, reverse polarity actuation voltage is applied to the piezoelectric actuator to shorten the PZT stack and open the valve.

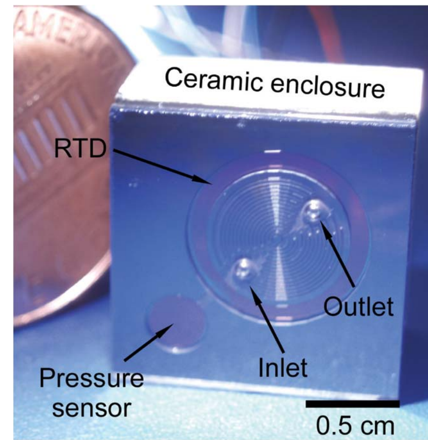

Fig. 6. Assembled valve looking from the glass side with U.S. penny. The pressure sensor cavity is connected to the inlet through a passage. The RTD is positioned on the backside of the silicon die. The valve has overall dimension of $1.5 \times 1.5 \times 1.1$ cm^3.

the constituents in Pyrex are various metal oxides, and HNO_3 is usually added to convert insoluble metal fluorides into soluble salts, thus reducing etch roughness [35]. The solution is diluted with water to tailor the etch rate. Following this shallow wet-etching, the mask is stripped. The wafer is then patterned again with Cr/Au and PR on both sides and subjected to a through-wafer etch. The wafer is placed in 49% HF to form the through holes for valve inlets and outlets. This time, no other chemicals are mixed with the solution to promote fast etch rate. The SOI wafer and the glass wafer are anodically bonded at 400 °C, and the wafers are diced to create the final valve die.

After the valve seats are fabricated, electrical connections are made to the sensors, and the devices are assembled with a piezoelectric (PZT) actuator stack and a glass-mica ceramic cap. The ceramic cap is machined from a bulk Macor material by conventional machining techniques. The PZT stack is bonded inside the Macor cap using Stycast 2850 FT cryogenic epoxy. Next, the valve is bonded to the PZT stack and the Macor cap using epoxy. The epoxy not only bonds, but also creates a layer that compensates for height differences between the actuator and ceramic housing, so the ceramic housing only needs to be machined within 200-μm tolerance.

At this stage, the assembly process can be varied to implement a normally open, partially open, or normally closed valve. (The same Si/glass die and Macor cap may be used for any of these three types of valves.) Fig. 5 shows this process. The general approach is to activate the PZT actuator to the desired closing voltage and then press it against the valve seat during the assembly process. In other words, to create a normally open valve, the PZT stack is energized at 100 V during the last assembly step so that it retracts when it is de-energized after assembly. During operation, the actuation voltage polarity is such that the stack expands. To create a normally closed valve, a stage is used to press down the valve seat until it comes into contact with the unactuated PZT stack. The voltage produced when PZT stack is pressurized is a good indication that contact is made. During operation the polarity of the voltage is such that the PZT stack retracts. A partially open valve is assembled by using a micrometer stage to drive the valve into contact, and then moving the stage away from the contact to the desired initial gap distance. The final valve structure measures $1.5 \times 1.5 \times 1.1$ cm^3 and is pictured in Fig. 6.

V. Experimental Results

Valve flow tests were conducted on normally open and normally closed valves at various pressures and temperatures down to 205 K. The pressure sensor was also tested across varying differential pressures at several temperatures. The embedded RTD was characterized from room temperature down to 50 K.

Normally open and normally closed valves were assembled by the method described in the previous section. They were tested at room temperature with N_2 gas flow. The N_2 gas was introduced to the inlet of the valve at the gauge pressure of 52 kPa, while the outlet was connected to a flow meter and vented to the atmosphere. The flow rate was measured as the valves were actuated from 0 to 40 V. In normally open valves, as the actuation voltage increases, the PZT stack expands to close the gap between the valve seats, decreasing the flow rate [Fig. 7(a)]. The flow rate changed from 200 mL/min at open state (0 V), down to below the measurement limit (< 1 mL/min) at closed state (40 V). The normally closed valve works by retraction of PZT when a reverse polarity voltage is applied. Therefore, the gap between the valve seats increases with the voltage, resulting in an increase in flow rate. This is illustrated in Fig. 7(b) with a curve in the opposite direction compared to that of Fig. 7(a), and it has a maximum flow rate of 115 mL/min at 40-V actuation. The hysteresis due to the piezoelectric

Authorized licensed use limited to: University of Michigan Library. Downloaded on September 8, 2009 at 22:10 from IEEE Xplore. Restrictions apply.

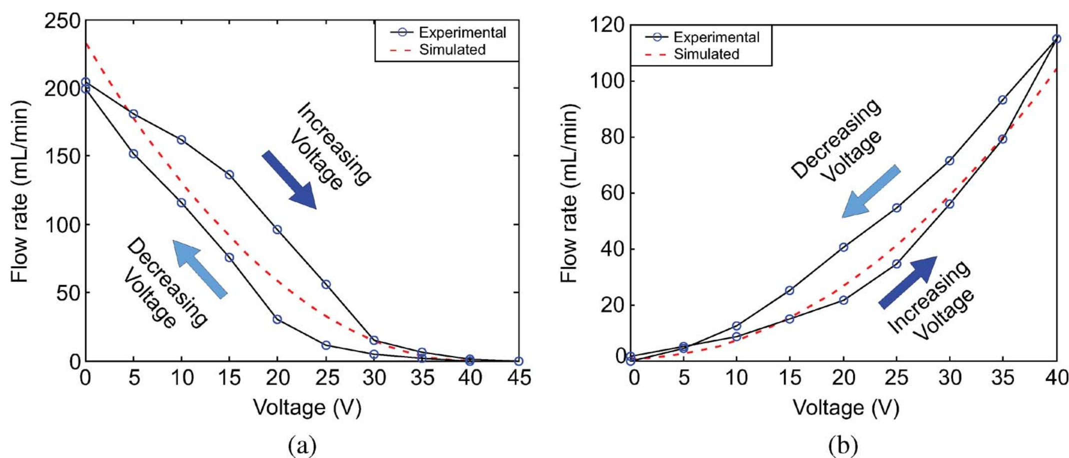

Fig. 7. Flow rates as a function of actuation voltage measured at room temperature compared with modeling results. Flow measurements of (a) normally open valve and (b) normally closed valve measured at differential inlet pressure of 52 kPa.

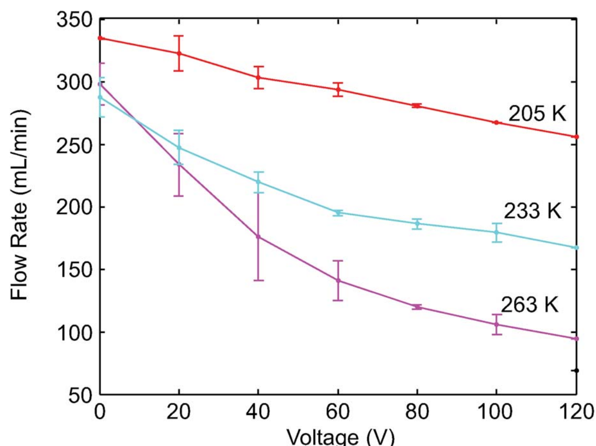

Fig. 8. Flow characteristic of normally open valve at different temperatures. The measurement was made at 34-kPa differential pressure with 160-kPa absolute inlet pressure. As temperature goes down, actuation of PZT has lesser effect on flow modulation, thus resulting a higher flow rate at a given actuation voltage. This is mainly due to a degraded piezoelectric performance at lower temperatures. Hysteresis of PZT actuation is represented as error bar here.

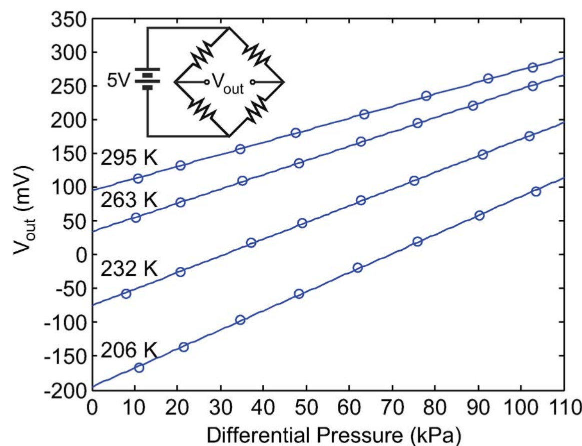

Fig. 9. Output voltage from piezoresistive pressure sensor at various differential pressures and temperature. The linearity of the pressure sensor was still good at low temperatures, however, the offset voltage and sensitivity of the sensor changes with varying temperature.

actuator can be seen in the flow rate variations for various set voltages.

A numerical model is presented with experimental results in Fig. 7, and shows good agreement. The model does not account for hysteretic behavior of PZT and assumes displacement is linearly proportional to the actuation voltage, and generally goes through the middle of the hysteresis curve. Uncertainties in actuator displacement and inlet and outlet hole size are responsible for discrepancies between the model and actual measurements.

The normally open valves were tested over a range of temperatures. The tests were conducted using He gas, and both the gas and the valve were cooled with a Cryomech AL60 GM cryocooler while the differential pressure was regulated at 34 kPa with an inlet pressure of 160 kPa. Fig. 8 represents the results by lines through the average value of hysteresis, while the hysteresis is represented as error bars. As temperature decreases, actuation of PZT has a lesser effect on flow modulation, resulting a higher flow rate at a given actuation voltage. When the valve is open (0 V), the flow rate is consistently at around 300 mL/min, but at 120-V actuation, flow rate increases from 95 mL/min at 263 K to 255 mL/min at 205 K.

Embedded pressure sensors were tested at various temperatures as the differential pressure across the valve was varied from 0 kPa up to above 100 kPa (Fig. 9). The pressure sensors were powered at 5 V as the differential output voltage was monitored. The linearity of the pressure sensor remains within $\pm 0.5\%$ across the range of pressure and temperature (206 K–295 K) tested. The slope of the line, which represents sensitivity of the sensor, increases from 356 to 563 ppm/kPa, and zero-pressure offset voltage decreases from 95 to -195 mV, as temperature decreases from 295 K to 205 K.

For characterization of the temperature sensor, the Pt RTD resistance was measured using a four-point method as the valve is cooled down to 50 K. A silicon diode cryogenic temperature sensor (Lake Shore Cryotronics, Inc.) was used as the temperature reference. Typical data from 300 K down to 50 K is shown in Fig. 10. The RTD response is very linear with the linearity error within $\pm 0.6\%$ down to 140 K, at which point the slope changed noticeably. Typical sensitivity is 0.29%/K above 140 K and 0.37%/K below.

Authorized licensed use limited to: University of Michigan Library. Downloaded on September 8, 2009 at 22:10 from IEEE Xplore. Restrictions apply.

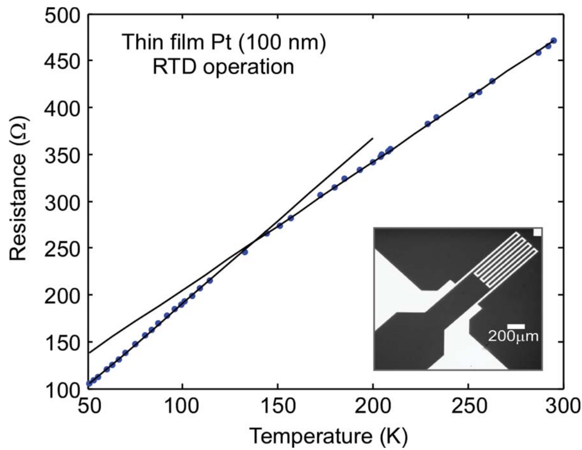

Fig. 10. Measured RTD resistance versus temperature change with best fit lines. The RTD shows bilinear behavior, with a sensitivity of 0.29%/K above 140 K and 0.37%/K below it.

VI. Discussion

In the flow modulation test, as shown in Fig. 8, as the temperature decreases, the PZT actuation has a decreased effect on flow rate modulation. This is mainly due to a degradation of the PZT stack that occurs because of the decreased piezoelectric constant at lower temperatures [28]. The decreased effectiveness in flow modulation is also apparent in decreased hysteresis. The piezoelectric constant is reduced by about 25% over the range of temperature tested. This is aggravated by the stiffness of the valve membrane $(3.8 \times 10^6\ \text{N/m})$ which required significant force during assembly to achieve good seal when valve is closed, which in turn resulted in reduced range of piezoelectric actuator displacement and range of flow modulation. A more compliant membrane structure, such as a corrugated membrane, may help improve the valve performance with added complexity in fabrication process. Change in stress on valve membrane due to thermal mismatch and thermal expansion mismatch between PZT actuator and Macor housing can also have effect on flow modulation.

While the scope of this paper is limited to gas flow modulation, in general, the structure of the valve isolates any electric connections from the flow path, and allows the use for liquid or mixed-phase heterogeneous coolant modulation which are likely to occur in cryogenic application. Liquid flow modulation has been explored at room temperature for drug delivery applications [36], [37]; additional exploration is ongoing and will be reported in the future.

The behavior of piezoresistive pressure sensor at different operating temperatures exhibit interesting trends. The slope of the plot (sensitivity) and zero-pressure offset voltage changes with temperature. The changes in sensitivity and offset voltage against temperature are plotted separately in Fig. 11 to illustrate this behavior. The sensitivity of the pressure sensor decreases with increasing temperature from 560 ppm/kPa at 206 K to 356 ppm/kPa at room temperature [Fig. 11(a)]. Temperature coefficient of the pressure sensitivity (TCS) is defined as fractional change in sensitivity per unit change in temperature. In our case, the TCS is -6507 ppm/K over the range of temperature tested, referenced to the sensitivity at room temperature. This behavior is almost entirely dominated by temperature coefficient of piezoresistive coefficient [38]. As presented by Kanda [39], the piezoresistive coefficient is a function of impurity concentration and temperature and assuming impurity concentration stays the same, the coefficient increases about 50% while temperature decreases from 298 K (25 °C) to 198 K (-75 °C). This corresponds well with the data shown in Fig. 11(a).

The offset voltage also changes as temperature reduces. Initial offset is introduced due to mismatched resistors. In our design of piezoresistors, the resistors that are transverse to the crystallographic axes are split into two segments and connected with metal lines to allow them to be placed close to the rim, while longitudinal resistors are one segment design. This geometric difference between transverse and longitudinal resistors can contribute to the mismatch in resistor values. The temperature effects on individual resistor can be represented as [40]

$$\Delta R = R_{T0}\alpha_R \Delta T + \Delta R\left(\pi(T), \sigma(T)\right) \tag{4}$$

where R_{T0} is resistance at the reference temperature, α_R is temperature coefficient of resistance, and the last term describes the change of resistance due to temperature dependence of the piezoresistive coefficient $\pi(T)$ and temperature-induced stress on membrane $\sigma(T)$. Temperature coefficient of offset (TCO) is defined as output voltage change as a fraction of supply voltage per unit change in temperature [38]. The typical TCO is 652 ppm/K over the temperature range tested. The temperature sensitivity of piezoresistive pressure sensors is well known and several compensation techniques exist [41]–[44]. However, in this particular application, since a temperature sensor is monolithically integrated with the valve and pressure sensor, it can be used to computationally correct the output. In this case, the accuracy of the derived pressure value depends on the accuracy of the temperature reading. Considering a worst case scenario, with 0.29%/K sensitivity and 0.6% error, the temperature sensor presented here can be off by 2 K. Multiplying this by the TCO and linearity error of the pressure sensor provides compounded pressure measurement error of 1370 ppm. Using the lowest pressure sensor sensitivity for the worst case scenario, the value translates to an upper bound of 3.8-kPa error.

The bilinear behavior of platinum RTD (Fig. 10) can be attributed to thermal expansion mismatch between silicon and glass, and the resulting stress on the membrane alters the resistivity. Although the coefficient of thermal expansion (CTE) of Pyrex is well matched to that of silicon in 0 °C–400 °C range [45], the CTE of silicon substantially decreases at low temperatures and turns to negative value below 140 K [33], while Pyrex maintains a CTE of 1.1 ppm/K even at 100 K [34]. This exerts compressive stress on the silicon membrane as temperature decreases, and alters resistivity of the thin-film platinum [46]. Although the temperature sensor exhibits some variation compared with standard platinum RTDs which provides linear response down to 70 K [26], the phenomenon is repeatable, and once calibrated, it can provide accurate temperature readings.

Authorized licensed use limited to: University of Michigan Library. Downloaded on September 8, 2009 at 22:10 from IEEE Xplore. Restrictions apply.

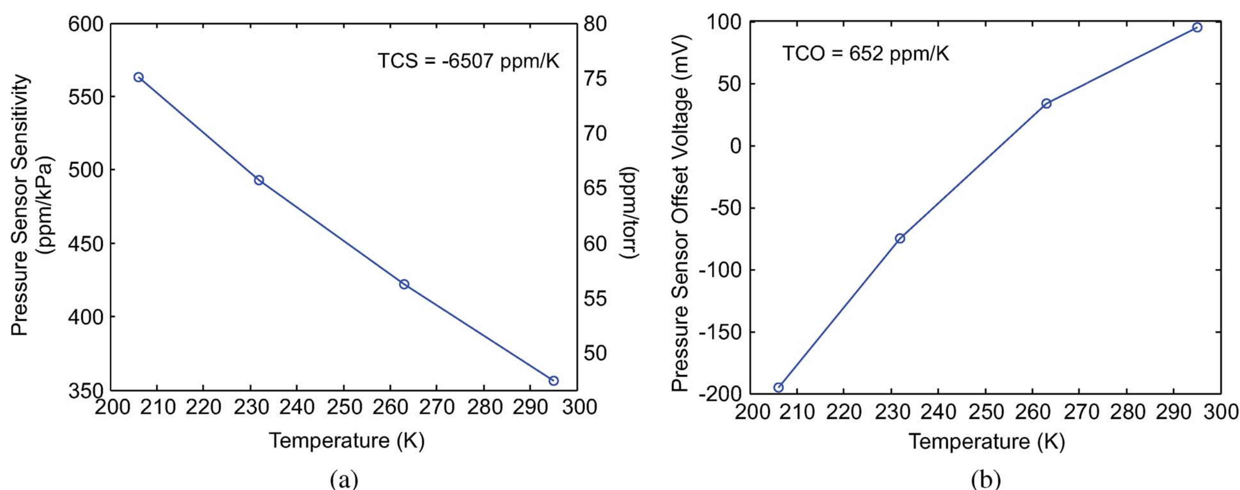

Fig. 11. Effect of temperature on piezoresistive pressure sensor. (a) Measured sensitivity of the pressure sensor decreases with increasing temperature with 356 ppm/kPa at room temperature. The sensitivity is plotted in both ppm/kPa and ppm/torr. The behavior is dominated by the temperature dependence of the piezoresistance factor. (b) Measured offset voltage also changes with temperature due to thermally induced stress on the membrane.

The measured temperatures and pressures values across a distributed cooling network may be gathered by a controller to properly adjust cooling rates to various parts of the surface to provide a minimal thermal gradient. The intention would be to adjust the valve opening with respect to current state. For example, when more cooling is required, the controller reduces actuation voltage to allow more coolant flow, and vice versa. This simplifies the control process without taking into account of complex hysteresis behavior of PZT, and allows graduated flow control. However, demonstration of such system is beyond the scope of this project.

VII. Conclusion

This effort has resulted in the successful fabrication of a suspended membrane piezoelectrically actuated ceramic-Si-glass microvalve with embedded sensors for use in distributed cooling applications. A perimeter augmentation scheme was used to overcome the limited displacement of PZT and provide large flow modulation. An assembly process was developed to allow for the creation of normally open, partially open, and normally closed valves. Both a normally open and normally closed valve were tested at room temperature, and allowed flow rates of up to 200 and 100 mL/min of N_2 at a differential pressure of 52 kPa. A normally open valve was tested at lower temperatures to below 200 K, and demonstrated the ability to modulate the flow over wide range of temperature. However, decreased flow modulation was observed due to the degraded actuation of the PZT stack. The stiff membrane suspension also contributes to limiting the range of flow modulation, but has a significant benefit of reducing dead volume by isolating the package cavity from the flow path.

Sensors were embedded with the valve to provide the necessary information for closed loop control of the valve. Piezoresistive pressure sensors were designed using implanted boron on a silicon diaphragm. The pressure sensor had a sensitivity of 356 ppm/kPa at room temperature, and the sensitivity increased with decreasing temperature, primarily due to change in piezoresistive coefficient with temperature. The pressure sensor also exhibited temperature dependent offset voltage drift that is mostly due to thermally induced stress on the membrane.

An RTD temperature sensor was fabricated using platinum on the backside of the fluidic channel. The temperature sensor exhibited the expected bilinear behavior of RTDs and had a sensitivity of 0.29%/K above 140 K and 0.37%/K below as it was tested down to 50 K. The RTD functions robustly down to cryogenic temperatures and should provide valuable information for feedback control and accurate calibration of the pressure sensor.

The valve presented here is designed to withstand up to 3 atm of differential pressure. The limitation comes from the structural integrity of the pressure sensor membrane at large differential pressures. The large blocking force of PZT actuator (> 500 N) allows operation at higher inlet pressure. With minor changes in pressure sensor dimensions, the valve is expected to work at higher pressure levels often demanded by Joule–Thompson systems.

It is worth noting that the valve can be scaled up or down according to desired flow rate; this can be done by changing the valve plate area or PZT stack height to allow for lower or higher flow rates. Additionally, specific unpowered flow rates can be set by assembling the valve with a nominal gap that meets application needs. Because the valve uses a membrane support structure which isolates any electrical connection from the flow path, it can be used for liquid flow modulation in various microfluidic applications. In addition, the valve can be deployed to operate in harsh environments, due to the ability to work across a wide range of temperatures and ceramic encapsulation.

Acknowledgment

The authors would like to thank the staff of the Lurie Nanofabrication Facility, and colleagues at the University of Michigan, particularly S.-H. Lee for valuable discussions on process-related issues.

Authorized licensed use limited to: University of Michigan Library. Downloaded on September 8, 2009 at 22:10 from IEEE Xplore. Restrictions apply.

REFERENCES

[1] D. J. Benford, M. J. Amato, J. C. Mather, S. H. Moseley, Jr., and D. T. Leisawitz, "Mission concept for the single aperture far-infrared (SAFIR) observatory," *Astrophys. Space Sci.*, vol. 294, no. 3/4, pp. 177–212, Dec. 2004.

[2] L. J. Hastings, D. W. Plachta, L. Salerno, and P. Kittel, "An overview of NASA efforts on zero boiloff storage of cryogenic propellants," *Cryogenics*, vol. 41, no. 11/12, pp. 833–839, Nov. 2001.

[3] S. C. Terry, J. H. Jerman, and J. B. Angell, "A gas chromatographic air analyzer fabricated on a silicon wafer," *IEEE Trans. Electron Devices*, vol. ED-26, no. 12, pp. 1880–1886, Dec. 1979.

[4] T. Ikehara, H. Yamagishi, and K. Ikeda, "Electromagnetically driven silicon microvalve for large-flow pneumatic controls," in *Proc. SPIE*, 1997, vol. 3242, pp. 136–144.

[5] Y. Shinozawa, T. Abe, and T. Kondo, "A proportional microvalve using a bi-stable magnetic actuator," in *Proc. IEEE Int. Workshop MEMS*, Nagoya, Japan, Jan. 1997, pp. 233–237.

[6] C. Fu, Z. Rummler, and W. Schomburg, "Magnetically driven micro ball valves fabricated by multilayer adhesive film bonding," *J. Micromech. Microeng.*, vol. 13, no. 4, pp. S96–S102, Jul. 2003.

[7] P. Dubois, B. Guldimann, and N. F. de Rooij, "High-speed electrostatic gas microvalve switching behavior," in *Proc. SPIE*, 2001, vol. 4560, pp. 217–226.

[8] J. Collier, D. Wroblewski, and T. Bifano, "Development of a rapid-response flow-control system using MEMS microvalve arrays," *J. Microelectromech. Syst.*, vol. 13, no. 6, pp. 912–922, Dec. 2004.

[9] N. Vandelli, D. Wroblewski, M. Velonis, and T. Bifano, "Development of a MEMS microvalve array for fluid flow control," *J. Microelectromech. Syst.*, vol. 7, no. 4, pp. 395–403, Dec. 1998.

[10] M. A. Huff, J. R. Gilbert, and M. A. Schmidt, "Flow characteristics of a pressure-balanced microvalve," in *Proc. IEEE Int. Conf. Solid-State Sens. Actuators (TRANSDUCERS)*, Yokohama, Japan, Jun. 1993, pp. 98–101.

[11] J. K. Robertson and K. D. Wise, "A nested electrostatically-actuated microvalve for an integrated microflow controller," in *Proc. IEEE Int. Workshop MEMS*, Oiso, Japan, Jan. 1994, pp. 7–12.

[12] M. J. Zdeblick and J. B. Angell, "A microminiature electric-to-fluidic valve," in *Proc. IEEE Int. Conf. Solid-State Sens. Actuators (TRANSDUCERS)*, Chicago, IL, Jun. 1987, pp. 437–439.

[13] C. A. Rich and K. D. Wise, "A high-flow thermopneumatic microvalve with improved efficiency and integrated state sensing," *J. Microelectromech. Syst.*, vol. 12, no. 2, pp. 201–208, Apr. 2003.

[14] P. W. Barth, C. C. Beatty, L. A. Field, J. W. Baker, and G. B. Gordon, "A robust normally-closed silicon microvalve," in *Solid-State Sens. Actuator Workshop*, Hilton Head Island, SC, Jun. 1994, pp. 248–250.

[15] P. W. Barth and G. Gordon, "High performance micromachined valve orifice and seat," U.S. Patent 5 333 831, Aug. 2, 1994.

[16] S. Messner, M. Muller, V. Burger, J. Schaible, H. Sandmaier, and R. Zengerle, "A normally-closed, bimetallically actuated 3-way microvalve for pneumatic applications," in *Proc. IEEE Int. Workshop MEMS*, Heidelberg, Germany, Jan. 1998, pp. 40–44.

[17] M. Kohl, D. Dittmann, E. Quandt, and B. Winzek, "Thin film shape memory microvalves with adjustable operation temperature," *Sens. Actuators A, Phys.*, vol. 83, no. 1–3, pp. 214–219, May 2000.

[18] E. H. Yang, C. Lee, J. Mueller, and T. George, "Leak-tight piezoelectric microvalve for high-pressure gas micropropulsion," *J. Microelectromech. Syst.*, vol. 13, no. 5, pp. 799–807, Oct. 2004.

[19] C. Lee, E. H. Yang, S. M. Saeidi, and J. M. Khodadadi, "Fabrication, characterization, and computational modeling of piezoelectrically actuated microvalve for liquid flow control," *J. Microelectromech. Syst.*, vol. 15, no. 3, pp. 686–696, Jun. 2006.

[20] J. M. Park, R. P. Taylor, A. T. Evans, T. R. Brosten, G. F. Nellis, S. A. Klein, J. R. Feller, L. Salerno, and Y. B. Gianchandani, "A piezoelectric microvalve for cryogenic applications," *J. Micromech. Microeng.*, vol. 18, no. 1, p. 015 023, Jan. 2008.

[21] J. M. Park, T. R. Brosten, A. T. Evans, K. Rasmussen, G. F. Nellis, S. A. Klein, J. R. Feller, L. Salerno, and Y. B. Gianchandani, "A piezoelectric microvalve with integrated sensors for cryogenic applications," in *Proc. 20th IEEE Int. Conf. MEMS*, Kobe, Japan, Jan. 2007, pp. 647–650.

[22] J. Franz, H. Baumann, and H.-P. Trah, "A silicon microvalve with integrated flow sensor," in *8th Int. Conf. Solid-State Sens. Actuators (TRANSDUCERS)*, Stockholm, Sweden, Jun. 1995, vol. 2, pp. 313–316.

[23] M. E. Piccini and C. B. Towe, "A shape memory alloy microvalve with flow sensing," *Sens. Actuators A, Phys.*, vol. 128, no. 2, pp. 344–349, Apr. 2006.

[24] S. K. Clark and K. D. Wise, "Pressure sensitivity in anisotropically etched thin-diaphragm pressure sensors," *IEEE Trans. Electron Devices*, vol. ED-26, no. 12, pp. 1887–1896, Dec. 1979.

[25] S. T. Cho, K. Najafi, and K. D. Wise, "Internal stress compensation and scaling in ultrasensitive silicon pressure sensors," *IEEE Trans. Electron Devices*, vol. 39, no. 4, pp. 836–842, Apr. 1992.

[26] C. J. Yeager, "A review of cryogenic thermometry and common temperature sensors," *IEEE Sensors J.*, vol. 1, no. 4, pp. 352–360, Dec. 2001.

[27] S. S. Courts, P. R. Swinehart, and C. J. Yeager, "A new cryogenic diode thermometer," in *AIP Conf. Proc.*, 2002, pp. 1620–1627.

[28] R. P. Taylor, G. F. Nellis, S. A. Klein, D. W. Hoch, J. Feller, P. Roach, J. M. Park, and Y. Gianchandani, "Measurements of the material properties of a laminated piezoelectric stack at cryogenic temperatures," in *Proc. 30th Int. Cryogenic Mater. Conf.*, Keystone, CO, Aug. 2005, pp. 200–207.

[29] T. R. Brosten, "Model and test of an actively controlled cryogenic micro valve," M.S. thesis, Dept. Mech. Eng., Univ. Wisconsin, Madison, WI, 2006. [Online]. Available: http://sel.me.wisc.edu/publications/theses/theses2.html

[30] T. R. Brosten, J. M. Park, A. T. Evans, K. Rasmussen, G. F. Nellis, S. A. Klein, J. R. Feller, L. Salerno, and Y. B. Gianchandani, "A numerical flow model and experimental results of a cryogenic micro-valve for distributed cooling applications," *Cryogenics*, vol. 47, no. 9/10, pp. 501–509, Sep./Oct. 2007.

[31] E. B. Arkilic, M. A. Schmidt, and K. S. Breuer, "Gaseous slip flow in long microchannels," *J. Microelectromech. Syst.*, vol. 6, no. 2, pp. 167–178, Jun. 1997.

[32] S. A. Kleinin *Engineering Equation Solver*. Madison, WI: Univ. Wisconsin, 2002. [Online]. Available: http://sel.me.wisc.edu/ees/new_ees.html

[33] A. P. Zhernov, "Lattice constant and coefficient of linear thermal expansion of the silicon crystal. Influence of isotopic composition," *Low Temp. Phys.*, vol. 26, no. 12, pp. 908–915, Dec. 2000.

[34] R. M. Buffington and W. M. Latimer, "Coefficients of expansion at low temperatures and thermodynamic applications of expansion data," *J. Amer. Chem. Soc.*, vol. 48, no. 9, pp. 2305–2319, Sep. 1926.

[35] A. T. Evans, J. M. Park, G. F. Nellis, S. A. Klein, J. R. Feller, L. Salerno, and Y. B. Gianchandani, "A low power, micro valve-regulated drug delivery system using a Si micro-spring pressurized balloon reservoir," in *Proc. 14th Int. Conf. Solid-State Sens., Actuators Microsyst. (TRANDUCERS)*, Tucson, AZ, 2007, pp. 359–362.

[36] A. T. Evans, J. M. Park, S. Chiravuri, and Y. B. Gianchandani, "Dual drug delivery device for chronic pain management using micromachined elastic metal structures and silicon microvalves," in *Proc. 21st IEEE Int. Conf. MEMS*, 2008, pp. 252–255.

[37] W. Kern and C. Deckert, "Chemical etching," in *Thin Film Processes*, J. L. Vossen and W. Kern, Eds. New York: Academic, 1978.

[38] S.-C. Kim and K. D. Wise, "Temperature sensitivity in silicon piezoresistive pressure transducers," *IEEE Trans. Electron Devices*, vol. ED-30, no. 7, pp. 802–810, Jul. 1983.

[39] Y. Kanda, "Graphical representation of the piezoresistance coefficients in silicon," *IEEE Trans. Electron Devices*, vol. ED-29, no. 1, pp. 64–70, Jan. 1982.

[40] U. Aljancic, D. Resnik, D. Vrtacnik, M. Mozek, and S. Amon, "Temperature effects modeling in silicon piezoresistive pressure sensor," in *Proc. IEEE Mediterranean Electrotechnical Conf.*, Cairo, Egypt, May 2002, pp. 36–40.

[41] G. Kowalski, "Miniature pressure sensors and their temperature compensation," *Sens. Actuators*, vol. 11, no. 4, pp. 367–376, May 1987.

[42] P. Kopystynski and E. Obermeier, "An interchangeable silicon pressure sensor with on-chip compensation circuitry," *Sens. Actuators*, vol. 18, no. 3/4, pp. 239–245, Jul. 1989.

[43] J. Bryzek, R. Mayer, and P. Barth, "New generation of disposable blood pressure sensors with digital on-chip laser trimming," in *Proc. IEEE Solid State Sens. Actuator Workshop*, Hilton Head Island, SC, Jun. 1988, pp. 121–122.

[44] T. Ishihara, K. Suzuki, S. Suwazono, M. Hirata, and H. Tanigawa, "CMOS integrated silicon pressure sensor," *IEEE J. Solid-State Circuits*, vol. SSC-22, no. 2, pp. 151–156, Apr. 1987.

[45] W. H. Ko, J. T. Suminto, and G. J. Yeh, "Bonding techniques for microsensors," in *Micromachining and Micropackaging of Transducers*, vol. 20. Amsterdam, The Netherlands: Elsevier, 1985, pp. 41–61.

[46] M. M. Nayak, N. Gunasekaran, A. E. Muthunayagam, K. Rajanna, and S. Mohan, "Diaphragm-type sputtered platinum thin film strain gauge pressure transducer," *Meas. Sci. Technol.*, vol. 4, no. 12, pp. 1319–1322, Dec. 1993.

Authorized licensed use limited to: University of Michigan Library. Downloaded on September 8, 2009 at 22:10 from IEEE Xplore. Restrictions apply.

Jong M. Park received the B.S. degree in electrical engineering (with honors) from Cornell University, Ithaca, NY, in 2003 and the M.S. and Ph.D. degrees in electrical engineering from the University of Michigan, Ann Arbor, in 2005 and 2009, respectively.

He is currently working as a Research Scientist with the Honeywell ACS Sensors and Wireless Laboratory, Plymouth, MN. His research interests include development of microvalves and pumps, integration of sensors and actuators, and microcooling systems.

Allan T. Evans received the B.S. degree in electrical engineering (with honors) in 2005 from Michigan State University, East Lansing, and the M.S. degree in electrical engineering in 2007 from the University of Michigan, Ann Arbor, where he is currently working toward the Ph.D. degree in electrical engineering in the Wireless Integrated Microsystems Laboratory.

His research focuses on the development of microvalves and pumps, integration of sensors and actuators, and implantable drug-delivery devices for the treatment of chronic pain.

Kristian Rasmussen, photograph and biography not available at the time of publication.

Tyler R. Brosten received the B.S. degree in mechanical engineering from Montana State University, Bozeman, and the M.S. degree in mechanical engineering from the University of Wisconsin, Madison. He is currently working toward the Ph.D. degree in mechanical engineering in the Magnetic Resonance Microscopy Laboratory, Montana State University.

He is currently with the Department of Mechanical Engineering, University of Wisconsin. His research focuses on the application of nuclear magnetic resonance microscopy to the study of stochastic dynamics occurring within transport in porous media.

Gregory F. Nellis received the B.S. degree from the University of Wisconsin, Madison, and the M.S. and Ph.D. degrees from the Massachusetts Institute of Technology, Cambridge.

He was with the Cryogenic Engineering Lab under the advisement of Prof. J. Smith. Following graduate school, he worked for several years with Creare Inc., on the development of turbo-Brayton cryogenic refrigeration systems. He is currently an Associate Professor in mechanical engineering with the University of Wisconsin. His current projects are related to pulse-tube, mixed-gas Joule-Thomson, and active magnetic regenerative refrigeration systems. He also carries out research related to thermal-fluid issues in advanced semiconductor manufacturing techniques, such as immersion and nanoimprint lithography. He teaches classes related to thermodynamics, heat transfer, and experimental measurement systems.

Sanford A. Klein is associated with the Solar Energy Laboratory, University of Wisconsin, Madison, and has been involved in many studies of solar and other types of energy systems. He has authored or coauthored over 150 publications relating to the analysis of energy systems. His current research interests include thermodynamics, alternative power generation systems, refrigerant properties, and alternative refrigeration systems. In addition, he is also actively involved in the development of engineering computer tools for instruction and research.

Yogesh B. Gianchandani received the B.S., M.S., and Ph.D. degrees in electrical engineering, with a focus on microelectronics and MEMS. He is presently a Professor at the University of Michigan, Ann Arbor, with a primary appointment in the Electrical Engineering and Computer Science Department and a courtesy appointment in the Mechanical Engineering Department. He is temporarily serving at the National Science Foundation, as the program director within the Electrical, Communication, and Cyber Systems Division (ECCS).

Dr. Gianchandani's research interests include all aspects of design, fabrication, and packaging of micromachined sensors and actuators and their interface circuits (http://www.eecs.umich.edu/~yogesh/). He has published approximately 200 papers in journals and conferences, and has about 30 U.S. patents issued or pending. He was a Chief Co-Editor of *Comprehensive Microsystems: Fundamentals, Technology, and Applications,* published in 2008. He serves several journals as an editor or a member of the editorial board, and served as a General Co-Chair for the IEEE/ASME International Conference on Micro Electro Mechanical Systems (MEMS) in 2002.

Authorized licensed use limited to: University of Michigan Library. Downloaded on September 8, 2009 at 22:10 from IEEE Xplore. Restrictions apply.